Loss of DDRGK1 Impairs IRE1α UFMylation to Promote IRE1α Degradation, ER Stress and Apoptosis in ATDC5 Cells

Xiao Yang
Shanghai Jiao Tong University School of Medicine Affiliated Ninth People's Hospital
Tangjun Zhou
Shanghai Jiao Tong University School of Medicine Affiliated Ninth People's Hospital
Ying Xia
Shanghai Jiao Tong University School of Medicine Affiliated Ninth People's Hospital
Haijun Tian
Shanghai Jiao Tong University School of Medicine Affiliated Ninth People's Hospital
Xiaofei Cheng
Shanghai Jiao Tong University School of Medicine Affiliated Ninth People's Hospital
Yu Cao
Shanghai Jiao Tong University School of Medicine Affiliated Ninth People's Hospital
Hui Ma
Shanghai Jiao Tong University School of Medicine Affiliated Ninth People's Hospital
An Qin
Shanghai Jiao Tong University School of Medicine Affiliated Ninth People's Hospital
Jie Zhao (profzhaojie@126.com)
Shanghai Jiao Tong University School of Medicine Affiliated Ninth People's Hospital
https://orcid.org/0000-0003-1000-5641

Research Article

Keywords: Spondyloepiphyseal dysplasia, DDRGK1, IRE1α, endoplasmic reticulum stress, apoptosis

Posted Date: October 19th, 2021

DOI: https://doi.org/10.21203/rs.3.rs-952431/v1

Abstract

Background

Spondyloepiphyseal dysplasia (SEMD) is a rare disease that is caused by the impaired development of cartilage. Although mutations in the *DDRGK1 domain-containing* (DDRGK1) gene have been found to be one of the causes of this disease, the underlying mechanism remains poorly understood. Here, we used the ATDC5 cell line to investigate the effects of the loss of DDRGK1 expression on chondrocyte physiology and cartilage development, with specific focus on endoplasmic reticulum (ER) stress.

Methods

DDRGK1-knockout ATDC5 cells were produced using the CRISPR/Cas9 technique, before their responsiveness to the loss of DDRGK1 was evaluated using Cell Counting Kit-8, and the apoptosis rate was measured using flow cytometry and Hoechst staining. ATDC5 chondrogenesis was evaluated using high-density pellet culture, followed by Alcian blueand terminal deoxynucleotidyl transferase dUTP nick end labeling staining. The potential interaction between DDRGK1 and inositol-requiring enzyme 1 α (IRE1α), in addition to the possible tagging of the ubiquitin-fold modifier 1 protein (UFMylation) and ubiquitylation of IRE1α, were measured using a co-immunoprecipitation assay. Expression of components in the ER stress and apoptosis signaling pathways was determined using reverse transcription-quantitative PCR and western blotting.

Results

DDRGK1 was found to interact with IRE1α on multiple sites, where it facilitates the UFMylation of IRE1α. Knocking out DDRGK1 expression led to increased IRE1α ubiquitylation and subsequent degradation, which in turn enhanced ER stress and activated the apoptosis signaling pathway. Loss of DDRGK1 also induced apoptosis whilst inhibiting the chondrogenic ability of ATDC5 cells. In addition, DDRGK1 knockout reduced the expression of SRY-box transcription factor 9 and aggrecan in ATDC5 pellets but aggravated ER stress.

Conclusions

Loss of DDRGK1 was concluded to impair the UFMylation of IRE1α, which then increases IRE1α ubiquitylation and degradation to promote chondrocyte apoptosis due to enhanced ER stress.

Background

Achondroplasia is a genetic disease that is caused by mutations in multiple genes and results in impaired cartilage growth and development[1]. The main characteristics of patients with Achondroplasia are short

stature and early-onset joint spinal degeneration[2–4]. In particular, one such unique type of Achondroplasia is Spondylo-epi-metaphyseal dysplasias (SEMD), which mainly affects the growth plates and epiphyses of the limbs and spine[5]. Patients with SEMD typically suffer from short stature, premature scoliosis and kyphosis, all of which are frequently observed with abnormal joint development in the limbs[5, 6]. Among the various genes that have been reported to cause Achondroplasia, a loss of function mutation (a homozygous c.408+1G>A donor splice site mutation) in the *DDRGK1 domain containing* (*DDRGK1*) gene is garnering interest in this research field[7–9].

Adetutu *et al* previously reported that the loss of DDRGK1 in zebrafish would lead to the reduced expression of the cartilage-specific protein SRY-box transcription factor 9 (SOX9), causing chondrogenic and osteogenic disorders[7]. In addition, previous studies found DDRGK1, which is also known as ubiquitin-fold modifier 1 protein (UFM1)-binding protein 1 with proteasome, COP9, initiation factor 3 domain (UFBP1), to be a key component of the ubiquitin-like protein family[8, 10]. As such, DDRGK1 is deeply involved in the process in which proteins get tagged with a UFM1 group, called UFMylation[11, 12]. Deletion of the *DDRGK1* gene has been demonstrated to inhibit the phosphorylation of inhibitor of NF-κB α subunit to protect it from ubiquitylation-mediated degradation in U2OS cells[13]. In plasma cells, loss of DDRGK1 blocked ER expansion and immunoglobulin production[14]. In addition, the DDRGK1 protein has also been shown to be involved in the activation of estrogen receptor α by regulating the activation of its downstream component activating signal co-integrator 1 (ASC1) and promoting it's UFMylation in MCF7 cells [15]. In tumor cells, including breast and liver cancer, DDRGK1 knockout was also revealed to induce endoplasmic reticulum (ER) stress and promote apoptosis[16].

Studies above have primarily focused on the expression of proteins related to growth, development and transcription, but little attention has been paid to the ER stress pathway. ER stress is a common phenomenon in cells following different physiological and pathological stimuli that affects the protein synthesis process[17]. There is accumulating evidence that chronic ER stress is associated with a variety of diseases, including cancer, neurodegeneration, diabetes, and proinflammatory diseases[18–21]. Unfolded protein response (UPR) is an adaptive response that promotes protein folding, processing, exporting and/or degradation during ER stress[17]. Although the initial stages of the UPR is a cytoprotective mechanism designed to restore homeostasis in the ER, chronic activation of the UPR can result in apoptosis[22, 23].

In our study, we explored the role of DDRGK1 in ER stress in ATDC5 chondrocytes. We probed for the sites of potential interaction between DDRGK1 and inositol-requiring enzyme 1 α (IRE1α) to explore the underlying UFMylation mechanism. In addition, *DDRGK1*-knockout ATDC5 cells were constructed to assess the intracellular mechanism and resulting phenotype further. Results from these *in vitro* studies revealed the specific mechanism of ER stress leading to apoptosis through DDRGK1-mediated IRE1α UFMylation in ATDC5, which may serve as a novel target for future research.

Methods

Reagents

Polymerase chain reaction (PCR) primers (Sangon Biotech Co., Ltd., Shanghai, China), Cell Counting Kit-8 (CCK-8; Dojindo Molecular Technologies, Inc., Kumamoto, Japan), TRIzol® reagent (Invitrogen; Thermo Fisher Scientific, Inc., Carlsbad, CA, U.S.A), PrimeScript™ RT Master Mix Kit (036a, Takara Biotechnology Co., Ltd., Dalian, China), TB Green® Premix Ex Taq™ Kit (420a, Takara Biotechnology Co., Ltd., Dalian, China), Phosphorylase Protease Inhibitor Mixture (Thermo Fisher Scientific, Inc., Waltham, Ma, U.S.A), DAPI (Sigma Aldrich, Merck KGaA, St Louis, MO, U.S.A), PVDF membranes (EMD Millipore, CA, U.S.A)Primary antibodies against myc-tag (cat. no. 71d10; rabbit mAb), B-cell lymphoma 2 (Bcl-2)-associated X (Bax; cat. no. d3r2m; rabbit mAb), IRE1α (cat. no. 14c10; rabbit mAb), protein disulfide isomerase (cat. no. c81h6; rabbit mAb), binding immunoglobulin protein (BiP; cat. no. c50b12; rabbit mAb), C/EBP homologous protein (CHOP; cat. no. l63f74; mouse mAb), Protein kinase RNA-like endoplasmic reticulum kinase (PERK; cat. no. c33e10; rabbit mAb), Caspase 3 (cat. no. 9662; rabbit mAb), Caspase 9 (cat. no. 9508; rabbit mAb), Cleaved Caspase 9 (cat. no. 9507; rabbit mAb), poly (ADP-ribose) polymerase (PARP; cat. no. 46d11; rabbit mAb) and β-actin (cat. no. d6a8; rabbit mAb) were purchased from Cell signaling Technology, Inc., Denver, MA, USA. Anti-IRE1α (cat. no. ab37073; rabbit mAb), Anti-gasdermin D (GSDMD; cat. no. ab219800; rabbit mAb), Anti-receptor-interacting protein (RIP; cat. no. ab202985; rabbit mAb), Anti-SOX9 (cat. no. ab185966; rabbit mAb) and Anti-UFM1 (cat. no. ab109305; rabbit mAb) were purchased from Abcam, Cambridge, UK. Anti-DDRGK1 (cat. no. 21445-1-AP; rabbit mAb) primary antibodies were purchased from ProteinTech Group, Inc., Chicago, IL, USA. Anti-Bcl-2 (cat. no. AF6139; rabbit pAb) and Anti-aggrecan (cat. no. DF7561; rabbit pAb) were purchased from Affinity Biosciences, Changzhou, China. Anti-hemagglutinin (HA)-tag (cat. no. abs137982; rabbit pAb) and anti-FLAG tag (cat. no. abs120265; rabbit pAb) primary antibodies were purchased from Absin Bioscience, Inc., Shanghai, China.

Culture of ATDC5 cells

ATDC5 chondrocytes are immortalized cell lines purchased from Shanghai Fuheng Biological Company (cat. no. FH0378). The cells were cultured in Dulbecco's modified Eagle medium F12 (DMEM/F12) with 5% fetal bovine serum (FBS) and 1% penicillin and streptomycin (Gibco, Thermo Fisher Scientific, Inc., Waltham, MA, USA) at 37°C with 5% CO^2.

DDRGK1 overexpression and knockout in ATDC5 cells

DDRGK1 overexpression (O/E; pcSLenti-CMV-DDRGK1-3xFLAG-PGK-Puro-WPRE) virus and O/E control (O/E-C; pcSLenti-CMV-3xFLAG-PGK-Puro-WPRE), in addition to viruses for DDRGK1 knockout, produced using the SgNC (GCACTACCAGAGCTAACTCA; pLenti-U6-spgRNA v2.0-CMV-EGFP) and SgDDRGK1(CCCCGGCGTCGGAGGGACTT; pLenti-U6-spgRNA v2.0(Ddrgk1)-CMV-EGFP) and Cas9 virus (pLenti-CMV-Puro-P2A-3Flag-espCas9_1.1), were purchased from Shanghai Heyuan Biological Company, Shanghai, China. For transfection, ATDC5 chondrocytes were seeded into a six-well plate at a density of 1x 10^5 cells per well. On day 2, O/E-C, O/E and Cas9 virus were added with a MOI of 20. On day 3, the media was changed, and the cells were screened with puromycin (cat. no. BS111; Biosharp, Hefei, China)

at a concentration of 5 μg/ml. On day 5, the O/E-C, O/E cells were determined by western blotting of DDRG1 and the Cas9 cells were then transfected with the SgNC or SgDDRGK1 viruses with a MOI of 20 for the second transfection. Among them, on day 7 the Cas9/SgNC and Cas9/SgDDRGK1 cell lines were then subjected to monoclonal culture. Firstly, 100 μl DMEM/F12 medium with 5% FBS and 1% penicillin and streptomycin were added to each well in a 96-well plate before 1,000 cells in 100 μl DMEM/F12 medium were added to A1 and mixed thoroughly. Subsequently, 100 μl DMEM/F12 medium with cells was transferred from A1 to B1, then repeatedly into H1. We then used an eight-channel pipette to transfer 100 μl medium with cells from the first line to the second line and finally into the last line in a 1:1 ratio. The cells were cultured in DMEM/F12 medium with 10% FBS and 1% penicillin and streptomycin at 37℃ with 5% CO^2.

High-density culture and pellet culture

To evaluate chondrocyte differentiation, 1.5x 10^5 ATDC5 cells (SgNC or SgDDRGK1) were resuspended in 10 μl medium and seeded into a 24-well plate. Cells were allowed to adhere at 37˚C for 1 h, before 0.5 ml DMEM/F12 medium containing 10 ng/ml insulin-transferrin-selenium (ITS) and 2% FBS was added. After 24 h at 37˚C, the cells were stimulated with or without thapsigargin (Tg, 6.25 nM; Apexbio; cat. no. B6614; Houston, TX, USA) and the medium was changed every 2 days. After 9 days at 37˚C, the micromasses were stained with alcian blue for 24 h at room temperature (RT).

For the pellet culture, 1.5x 10^7ATDC5 cells (SgNC or SgDDRGK1) were centrifuged as a pellet in the bottom of a 15-ml centrifuge tube, which was filled with the Mesenchymal Stem Cell Chondrogenic Differentiation Medium (Cyagen Biosciences, Inc., Santa Clara, CA, USA). The medium was refreshed every 3 days. After 21 days of culture at 37˚C, the pellets were collected via tweezer and fixed in 4% paraformaldehyde (PFA) for 5 h at RT and then embedded in optimal cutting temperature compound (Sakura Finetek USA, Inc.). The pellets were then stored at -80˚C overnight and cut to a 20-μm thickness using a freezing microtome (Leica Microsystems GmbH)

RNA extraction and reverse transcription-quantitative PCR (qPCR) analysis

According to the manufacturer's protocols, TRIzol Reagent was used to isolate total RNA from tissues and cells. First strand complementary DNA (cDNA) was reverse transcribed from the extracted RNA using a PrimeScript™ RT Master Mix Kit (036a, Takara Biotechnology Co., Ltd., Dalian, China). TB Green Premix Ex Taq Kit (Takara bio, Inc., Otsu, Japan) was used to perform qPCR in the Applied Biosystems QuantumStudio 6 Flex Real-Time PCR system (Thermo Fisher Scientific, Inc., Waltham, MA, USA) per the following conditions: Denaturation at 95˚C for 30 sec; 40 cycles of 95 ˚C for 3 sec and 60 ˚C for 34 sec; and then 95 ˚C for 15 sec, 60 ˚C for 60 sec and finally, 95 ˚C for 15 sec. Specific primer pairs were designed using NCBI blast and the sequences are provided in Table 1. GAPDH gene expression was used as the internal controls. Target gene expression levels were determined using the $2^{-\Delta\Delta Cq}$ method[24].

Table 1
Primer sequences used for RT-qPCR.

Gene	Accession Number		5’→3’
IRE1α	NM_023913.2.	F	CAATCGTACGGCAGTTGGAG
		R	CTCCCGGTAGTGGTGTTTCT
BiP	NM_022310.3	F	GAAAGGATGGTTAATGATGCTGAGAAG
		R	GTCTTCAATGTCCGCATCCTG
CHOP	NM_007837.4	F	CATACACCACCACACCTGAAAG
		R	CCGTTTCCTAGTTCTTCCTTGC
BAX	NM_007527.3	F	CTGGATCCAAGACCAGGGTG
		R	CCTTTCCCCTTCCCCCATTC
BCL2	NM_009741.5	F	AGCATGCGACCTCTGTTTGA
		R	GCCACACGTTTCTTGGCAAT
Col2a1	NM_001113515.2	F	AGGTGTTCGAGGAGACAGTG
		R	CAACAATGCCCCTTTGACCA
SOX9	NM_011448.4	F	TGAAGATGACCGACGAGCAG
		R	GGATGCACACGGGGAACTTA"
DDRGK1	NM_029832.2	F	GAGCACGAGGAGTACCTGAAA
		R	TCCTGAGTCCTTAGGCCCATC

Cell viability test

CCK-8 was used to evaluate cell viability of DDRGK1 O/E and O/E-C, SgNC and SgDDRGK1 ATDC5 cells. The cells were seeded into a 96-well plate at a density of 3,000 cells per well the day before treatment with thapsigargin (Tg, 6.25 nM; Apexbio; cat. no. B6614; Houston, TX, USA) for 24, 48, 72 and 96 h at 37˚C. ATDC5 chondrocytes were cultured in DMEM/F12 supplemented with 5% FBS and 1% penicillin and streptomycin at 37℃ with 5% CO^2. The cell culture medium was changed every 2 days. At the end of the experiment, fresh 100 μl medium containing 10 μl CCK-8 reagent was added into each well prior to incubation at 37˚C for 1 h. Medium containing the CCK-8 reagent added to wells without cells was designated as the blank group whereas untreated cells were designated as the control group. Absorbance at 450 nm (as measured by optical density; OD) in each well was measured using the Infinite M200 Pro microplate reader (Tecan Group, Ltd., Mannedorf, Switzerland).

Co-immunoprecipitation (Co-IP) assay

293T cells or SgNC and SgDDRGK1 ATDC5 chondrocytes were transfected with Flag-PLVC, Flag (HA)-DDRGK1, HA (Flag)-IRE1α SgNC, HA (Flag)-IRE1α ΔC, HA (Flag)-IRE1α ΔN, HA (Flag)-IRE1α luminal domain (LD), HA (Flag)-IRE1α cytosolic domain (ICD), Flag-IRE1α Del468, Flag-IRE1α Del469 and HA-UFM1 plasmids (synthesized, purchased from Shanghai Ai Bosi Biological Technology Co., Ltd.) using lipofectamine 3000 (cat. no. L3000015; Thermo Fisher Scientific, Inc., Waltham, MA, USA) before they were washed three times with phosphate-buffered saline (PBS). Subsequently, 1.2 ml RIPA lysis buffer with 12 µl protease inhibitor, protein phosphatase inhibitor A + B and PMSF (Roche Diagnostics GmbH, Mannheim, Germany) was added to the cells and incubated for 20 min at 4˚C. After centrifugation at 13000 x g for 15 min at 4˚C, to 200 µl of the protein supernatant 50 µl protein loading buffer (5X) was added and this sample was boiled at 99˚C for 10 min whereas the remaining 1,000 µl of the protein supernatant was incubated with 30 µl Flag-tagged (or HA-tagged) magnetic beads (Sigma-Aldrich, Merck KGaA, St Louis, MO, U.S.A.) at 4˚C overnight. The next day, the magnetic beads were isolated from protein supernatant by Magnet Frame (Selleck Chemicals, China), and then washed three times with Tris-buffered saline (TBS) at 4˚C for 10 min with protease inhibitor, protein phosphatase inhibitor A + B and PMSF before being boiled at 99˚C for 5 min with 50 µl 1X RIPA lysis bufferto extract the proteins.

UFM1 modification assay

293T cells were transfected with Flag-PLVC, Flag-IRE1α, HA-UFM1, Myc-DDRGK1, Myc-UFM1 specific ligase 1 (UFL1) and Myc-UFM1-conjugating enzyme 1 (UFC1) or were transfected with Flag-PLVC, Flag-IRE1α, HA-UFM1, si-DDRGK1, Myc-UFL1 and Myc-UFC1 plasmids (synthesized, purchased from Shanghai Ai Bosi Biological Technology Co., Ltd.) using lipofectamine 3000 (cat. no. L3000015; Thermo Fisher Scientific, Inc., Waltham, MA, USA). After culturing for 48 h, cells were washed three times with PBS before the protein samples were extracted using 1.2 ml NETT. In total, 200 µl lysate was used as input and the remaining 1,000 µl was incubated with 30 µl Flag-tagged magnetic beads at 4˚C overnight. The next day, the beads were boiled with 50 µl 1X loading RIPA lysis buffer at 99˚C for 10 mins and finally subjected to 10 or 12.5% SDS-PAGE electrophoresis buffer followed by immunoblot analysis.

Ubiquitylation modification assay

293T cells were transfected with Flag-PLVC, HA-IRE1α and Flag-Ubiquitin, Flag-PLVC and Flag-Ubiquitin or with Flag-PLVC, Flag-IRE1α, HA-UFM1, Myc-DDRGK1, Myc-UFL1, Myc-UFC1 and Flag-Ubiquitin plasmids (synthesized, purchased from Shanghai Ai Bosi Biological Technology Co., Ltd.) using lipofectamine 3000 (cat. no. L3000015; Thermo Fisher Scientific, Inc., Waltham, MA, USA). After culturing for 40 h, cells were stimulated with MG132 (10µM; cat. no. S2619; Selleck Chemicals, China) for 8 h at 37˚C and then washed three times with PBS. After using 1.2 ml NETT to extract protein, 200 µl lysate was used as input whilst the remaining 1,000 µl samples were incubated with 30 µl HA-tagged magnetic beads at 4˚C overnight. The samples were then boiled at 99˚C for 10 min and finally subjected to 10 or 12.5% SDS-PAGE electrophoresis buffer followed by immunoblot analysis.

Hoechst stain for apoptosis

SgNC and SgDDRGK1 ATDC5 chondrocytes were seeded into a six-well plate at a density of 3 x 10^4 cells per well. The next day, cells were fixed with 4% PFA for 5 min at RT and washed with PBS three times. Hoechst stain solution (5μg/ml; Beyotime Institute of Biotechnology) were added for 5 min at RT and washed with PBS for three times, before the cells were imaged using fluorescence microscopy (Leica Microsystems GmbH) at x10 and x20 magnification.

Flow cytometry

According to the manufacturer's protocol, flow cytometry was used to evaluate the effect of 1x 10^6 DDRGK1 overexpression and knockout cells on the apoptosis rate after staining with Annexin V, 633 Apoptosis Detection Kit (cat. no. AD11; Dojindo Molecular Technologies, Inc., Kumamoto, Japan). FACSCalibur Flow Cytometer (BD Biosciences) was used to count ≥20,000 events. The percentage of cells in the upper right quadrant (Q2; annexin V and PI positive) and the lower right quadrant (Q3: annexin V positive and PI negative) was used to quantify the apoptosis rate.

Western blotting

Total protein was extracted from the ATDC cells using RIPA lysis buffer supplemented with phosphatase and protease inhibitors (Roche, Basel, Switzerland). The protein was quantified by BCA assay (Thermo Fisher Scientific, Inc.) and then equal amounts of the extracted protein were separated (20-30 μg) in a 4-20% SurePAGE™ gel and transferred onto 0.22μm PVDF membranes (MilliporeSigma). The membranes were blocked with 5% bovine serum albumin (BSA)-TBS-Tween 20 (TBST) at room temperature for 1 h and then incubated with primary antibodies (diluted 1:1,000 in 5% BSA) against myc-tag, Bax, IRE1α, PDI, BiP, CHOP, PERK, Caspase 3, Caspase 9, Cleaved Caspase 9, PARP, β-actin, GSDMD, RIP, SOX9, UFM1, DDRGK1, Bcl-2, Aggrecan, HA-tag, FLAG-tag at 4˚C overnight. The next day, all membranes were washed with TBST and incubated with the anti-rabbit IgG (H + L) (dylight)™ secondary antibody (cat. no. 5151; DyLight™ 800 4X PEG Conjugate; Cell Signaling Technology, Inc.; 1:5,000) at room temperature for 1 h in the dark. The membranes were extensively washed in TBST before the protein bands were detected using a Li-Cor Odyssey Fluorescence Imaging System (Li-COR Biosciences, Lincoln, NE, USA). Intensity of the protein immunoreactive bands was measured using the Image Pro Plus 6.0 software (Media Cybernetics, Inc.) with intensity of the β-actin band used as internal reference.

Immunofluorescence staining

The pellet culture was sectioned into 20-μm thick frozen sections for histological evaluation. The frozen sections were washed with PBS three times at RT to remove the OCT solution and stained with Safranin O-Fast green (cat. no. G1053; Servicebio, Wuhan, China) and hematoxylin and eosin dyes (cat. no. G1001; Servicebio, Wuhan, China) at RT for 2-5 min, in accordance with the manufacturer’s protocols. For immunofluorescence staining, the frozen sections were defrosted at room temperature for 30 min, washed with PBS three times and incubated at 37˚C in an antigen retrieval buffer (Roche Diagnostics, Basel, Switzerland) for 30 min. An auto-fluorescence quenching agent was added to the sections for 5 min at RT and blocked with blocking buffer at room temperature for 30 min. The sections were then incubated with primary antibody (1:100 dilution) IRE1α (cat. no. ab37073; rabbit mAb), SOX9 (cat. no.

ab185966; rabbit mAb), CHOP (cat. no. I63f74; mouse mAb), DDRGK1 (cat. no. 21445-1-AP; rabbit mAb) and Anti-aggrecan (cat. no. DF7561; rabbit pAb) in a wet box at 4˚C overnight. The next day, the slices were washed with PBS and incubated with the Alexa-Fluor® 594-conjugated secondary antibody (cat. no. 8889; anti rabbit; 1:500; Cell Signaling Technology, Inc., Danvers, MA, USA) in the dark at room temperature for 50 min. The sections were washed with PBS and incubated with a DAPI solution (Sigma Aldrich, Merck KGaA, St. Louis, MO, USA) in the dark for 10 min at RT to stain the nuclei. After a final wash with PBS, the samples were air-dried and sealed with anti-fluorescence quenching tablets. A fluorescence image was then taken using the Leica DM4000 B fluorescence microscope (Leica Microsystems GmbH) at a x10 magnification, and the integrated optical density (IOD)/DAPI was measured by Image Pro Plus 6.0 software (Media Cybernetics, Inc.).

TUNEL assay

The pellet frozen sectons were washed with PBS three times at RT to remove the OCT solution and stained with Fluorescein (FITC) Tunel Cell Apoptosis Detection Kit (cat. no. G1501; Servicebio, Wuhan, China) according to the manufacturer's protocols. A fluorescence image was then taken using the Leica DM4000 B fluorescence microscope (Leica Microsystems GmbH) at a x10 magnification, and the TUNEL-positive cells was measured with the following formula: TUNEL-positive cells/total number of cells × 100% by Image Pro Plus 6.0 software (Media Cybernetics, Inc.).

Statistical analysis

Three independent experiments were performed on all data. The data were expressed as the mean ± standard deviation. SPSS 19.0 software (IBM Corp, Armonk, NY, USA) was used to perform two-tailed unpaired Student's t-test or one-way ANOVA with Tukey's post hoc test on the data. Unless otherwise specified, $P<0.05$ was considered to indicate a statistically significant difference.

Results

Loss of DDRGK1 in ATDC5 cells led to ER stress and apoptosis

To explore the underlying mechanism of DDRGK1 on chondrogenesis, we constructed DDRGK1-O/E and SgDDRGK1 ATDC5 cell lines and then used Tg (6.25 nM) to simulate ER stress. According to results from the CCK-8 assay, the viability of SgDDRGK1 cells was found to be significantly reduced compared with that in SgNC cells at all timepoints tested (Figure 1A). In addition, Tg potently reduced cell viability in both SgNC and SgDDRGK1 cells (Figure 1A). Loss of DDRGK1 also caused cell swelling, where the amount of space between cells was significantly increased (Figure 1B). Following treatment with Tg, SgDDRGK1 cells began to exhibit features of cell death, with the cell shape appearing to be stretched and Hoechst staining revealing significantly increased nuclear pyknosis (Figure 1D, F). According to flow cytometry analysis, the SgDDRGK1 condition exhibited more apoptotic cells, but with Tg treatment the apoptosis rate was higher in SgDDRGK1 cells compared with that in SgNC cells (Figure 1C, E). Following western

blot analysis to characterize the intracellular mechanism further, we next found increased Bax expression and decreased Bcl-2 expression after Tg treatment in both SgNC and SgDDRGK1 cells. Furthermore, the Bcl-2/Bax ratio was significantly decreased in SgDDRGK1 cells compared with SgNC cells with Tg(Figure 1G,H). The protein levels of end-stage apoptosis markers cleaved-caspase 3 and cleaved-PARP were also found to be increased in SgDDRGK1 cells compared with SgNC cells, which were increased further by Tg treatment. However, there were no changes in the expression of the pyroptosis marker GSDMD or the necrosis marker RIP after Tg addition (**Supplementary Figure 1a**), suggesting that the loss of DDRGK1 led to cell apoptosis through the Bax/Bcl-2/Caspase 3 signaling pathway, instead of pyroptosis or necrosis (Figure 1G, H).

Loss of DDRGK1 impaired chondrogenesis but DDRGK1 overexpression did not affect this ability

During the period of chondrogenesis, ATDC5 cells cultured in high density (~15 million cells/ml) secretes high quantities of extracellular matrix (ECM) covering the cells[25]. The most important component of this type of ECM is acid mucopolysaccharide, which can be stained with Alcian blue[26]. After 5 days of high-density chondrogenic culture SgDDRGK1 cells showed no difference compared with SgNC cells in terms of Alcian blue staining, with only slight staining without significance (Figure 2C-E). However, after a further 2 days staining was markedly lower in SgDDRGK1 cells compared with that in the SgNC cells (Figure 2C, E). On day 9, the structure of the cell mass became fractured with the ECM detached and apoptotic cells observed in SgDDRGK1 cells (Figure 2C, E). After Tg addition as the ER stress trigger, the structure of ECM in SgNC cells broke and the quantity was decreased whereas those in SgDDRGK1 cells were deteriorated more compared with SgNC cells (Figure 2F **and Supplementary Figure 1b**). This suggest that the loss of DDGK1 impaired the chondrogenesis ability of ATDC5 cells in high-density culture.

To verify this phenotype further, we used pellet culture to evaluate the chondrogenesis ability of ATDC5 cells in a three-dimensional context. After pellet culture for 21 days, ATDC5 cells became a cartilage-like cell mass abundant with ECM, where the SgDDRGK1 cells exhibited markedly less Alcian blue staining compared with that in SgNC cells, the difference of which was particularly striking in the central area of the pellet (Figure 2G **and Supplementary Figure 1c**). According to Safranin O-Fast green staining, the majority of the SgNC cell pellet stained with Safranin O, but the central part of the SgDDRGK1 cell pellet was only stained with Fast green, suggesting that the chondrogenesis ability was impaired (Figure 2H **and Sup. Figure 1D**).

With the finding that the loss of DDRGK1 expression is detrimental to ATDC5 cell chondrogenesis, we subsequently constructed the O/E cell line, which overexpresses DDRGK1 (O/E-C as a control), to assess its effects on this ability. However, overexpression of DDRGK1 exerted no effects on ATDC5 cell chondrogenesis in high density culture, since no changes were observed in Alcian blue staining (Figure 2A, B **and Supplementary Figure 2a**), In addition, the cell viability of O/E cells was found to be lower compared with that in the O/E-C cells (**Supplementary Figure 2b**). Using Tg as the ER stress trigger to

initiate the apoptosis pathway in both cells, we found no difference in the apoptosis rate of both O/E and O/E-C cells (**Supplementary Figure 2d**). Using western blotting, although we detected increased DDRGK1 expression and slightly decreased levels of BiP expression and cleaved-caspase 3, overexpression of DDRGK1 conferred no effects on IRE1α, CHOP or cleaved-PARP protein levels during the induction of apoptosis via Tg treatment (**Supplementary Figure 2c**).

DDRGK1 interacts with IRE1α on multiple sites

DDRGK1 is localized to the ER and participates in the UPR, which regulates ER stress partly through the IRE1α/ER-associated degradation (ERAD) pathway[27]. Therefore, we transfected 293T cells with Flag-IRE1α and used the Flag-tagged beads to pull down any interacting protein partners, from which DDRGK1 was detected (Figure 3A). Co-transfecting the cells with either Flag-DDRGK1 and HA-IRE1α (or Flag-IRE1α and HA-DDRGK1) resulted in the interaction between both proteins being detected using Flag-tagged beads (Figure 3B). To study the mechanism underlying this interaction further, we constructed the following four plasmids each encoding truncated versions of IRE1α for transfection: the transmembrane part named ΔC, which contains amino acid residues 1-469; the transmembrane part named ΔN, which has amino acid residues 19-439 deleted; the ER luminal domain named LD, which consists of amino acids 1-440; and the cytosol domain named ICD, which consists of amino acids 468-977 (Figure 3C). After co-transfecting these constructs into 293T cells with Flag-DDRGK1, we found that DDRGK1 interacted with IRE1α on multiple sites, since we detected interaction between Flag-DDRGK1 and IRE1α ΔC, IRE1α ΔN and IRE1α ICD but not IRE1α LD (Figure 3D, E). We noted that the IRE1α ΔC and the IRE1α ICD variants share the same amino acids, namely residues 468 and 469. Therefore, we constructed plasmids encoding the Del468 (Residue 468 deletion) and Del469 (Residue 469 deletion) IRE1α variants for transfection before co-immunoprecipitation. None of these two amino acids were found to be essential for interaction between DDRGK1 and IRE1α, since deletion of either of these two amino acids did not disrupt this interaction (Figure 3F).

DDRGK1 stabilizes the interaction between IRE1α with UFM1 which is disrupted by the loss of DDRGK1 expression

Since DDRGK1 is a key member of the UFMylation family and participates in the UFMylation pathway[9], we next explored this relationship. We transfected 293T cells with Flag-IRE1α or HA-UFM1, following which we detected the interaction between IRE1α and UFM1 (**Supplementary Figure 3a, b**). Not limited to intrinsic interactions, cells transfected with both plasmids also yielded UFM1/IRE1α complexes derived exogenously using Flag-tagged beads (Figure 3G). To decipher the function of DDRGK1 in the connection between IRE1α and UFM1 further, we constructed a poly-UFMylation system based on the co-immunoprecipitation concept. The 293T cells were transfected with the following two combinations of plasmids: Flag-IRE1α, HA-UFM1, Myc-UFL1, Myc-UFC1 and Myc-DDRGK1; or Flag-IRE1α, HA-UFM1, Myc-UFL1, Myc-UFC1 and si-DDRGK1. Expression of these proteins, especially UFM1, UFL1 and UFC1, was necessary for the successful establishment of this poly-UFMylation system, since Flag-tagged beads

could only detect UFMylated IRE1α when UFM1, UFL1 and UFC1 were co-expressed together. Presence of DDRGK1 was found to strengthen IRE1α UFMylation whereas DDRGK1 knockdown impaired IRE1α UFMylation (Figure 4A, B). Using SgDDRGK1 and SgNC ATDC5 cells, we transfected them with Flag-IRE1α or HA-UFM1. We observed that Flag-tagged beads pulled down reduced quantities of UFM1 compared with those in SgNC cells (**Supplementary Figure 3C**). By contrast, HA-tagged beads could not pull down any IRE1α in SgDDRGK1 ATDC5 cells (**Supplementary Figure 3d**). In general, DDRGK1 stabilizes the interaction between IRE1α to UFM1, facilitating the UFMylation of IRE1α in ATDC5 cells.

Loss of DDRGK1 expression led to the degradation of IRE1α and aggravation of ER stress

We found that the mRNA expression of IRE1α did not change in SgDDRGK1 and SgNC cells following DDRGK1 knockout (**Supplementary Figure 4a, b**). However, on the protein level, IRE1α expression was decreased in SgDDRGK1 cells compared with SgNC cells. In addition, after treating the cells with cycloheximide (CHX) to inhibit the synthesis of proteins, although IRE1α expression was decreased in both SgDDRGK1 and SgNC cells, IRE1α expression became almost negligible in SgDDRGK1 cells (Figure 4C). By contrast, co-treating the cells with MG-132 and CHX to also inhibit proteasome activity resulted in the partial rescue of IRE1α expression in both SgDDRGK1 and SgNC cells (Figure 4C). Unlike MG132, co-treatment of cells with CHX and chloroquine (Chlq), a lysosome and autophagy inhibitor, did not rescue IRE1α expression in both SgDDRGK1 and SgNC cells (Figure 4D). This suggests that the degradation of IRE1α in SgDDRGK1 cells is mediated through the ubiquitin-associated proteasome degradation pathway instead of the lysosome-autophagy system. Subsequently, treatment of ATDC5 cells with MG-132 alone for 0, 4 and 8 h resulted in the time-dependent poly-ubiquitylation of IRE1α (Figure 4E). An “up-shifting” of the bands was observed, where the magnitude was greater in SgNC cells compared with that in SgDDRGK1 cells (Figure 4E).

IRE1α is one of the three transmembrane proteins on the ER membrane that can regulate ER stress in cells[28]. As such, degradation of IRE1α lead to increased expression of the chaperone protein BiP. (Figure 4F **and Supplementary Figure 4c**). Using Tg as the ER stress trigger, we observed that IRE1α expression was increased (Figure 4F **and Supplementary Figure 4b**), with increased production of BiP, moreover, the increased level of BiP increased more in SgDDRGK1 cells compared with SgNC cells (Figure 4F **and Supplementary Figure 4c**). The excessive accumulation of the unfolded proteins activated another UPR pathway: PERK/CHOP pathway. Activated PERK increased the translocation of CHOP into the nucleus (Figure 4F **and Supplementary Figure 4d**), which would induce ER stress-mediated apoptosis. The mRNA expression levels of Bax were increased in SgDDRGK1 cells compared with SgNC cells and even more deteriorated following with Tg treatment. This coincided with the decreased Bcl-2 expression observed in SgDDRGK1 cells, which was decreased further following Tg treatment (**Supplementary Figure 4e, f**).

Ubiquitylation of IRE1α led to degradation but IRE1α UFMylation antagonizes this *in vitro*.

To verify that IRE1α was can be ubiquitylated we co-transfected the 293T cells with HA-IRE1α and Flag-Ubiquitin followed by MG-132 treatment for 12 h. We found that incubating the samples with HA-tagged beads pulled down IRE1α that revealed poly-ubiquitylated bands (Figure 5A). We also constructed the Flag-Ubiquitin plasmid and transfected this into 293T cells for co-immunoprecipitation, which was found to successfully pull down IRE1α using Flag-tagged beads (Figure 5B).

To further decipher the relationship between Ubiquitylation and UFMylation. we subsequently transfected 293T cells with Flag-IRE1α, HA-UFM1, Myc-UFL1, Myc-UFC1, Myc-DDRGK1 and HA-ubiquitin to construct the poly-ubiquitylation and poly-UFMylation systems. We observed that ubiquitylation of IRE1α was decreased whilst the levels of UFMylated-IRE1α were increased with overexpression of Myc-DDRGK1 (Figure 5C).

Loss of DDRGK1 impaired chondrogenesis, activated ER stress and induced the apoptosis in the ATDC5 pellet culture

Based on observations from the present study of the mechanism underlying the effects of DDRGK1 on ER stress, there is accumulating evidence that the impairment of chondrogenesis was partially due to the apoptosis of ATDC5 cells, which may be theoretically associated with the clinical manifestations of SEMD. To test this hypothesis, we used the pellet culture to form an *in vitro* cartilage structure for mechanistic exploration. Sg DDRGK1 ATDC5 cells exerted significant influence on chondrogenesis, since the expression of important chondrocyte markers, including aggrecan[29] and SOX9[30], were decreased according to immunofluorescence and western blotting results in SgDDRGK cells compared with SgNC cells(Figure 6A,C). moreover, we could also detect a downregulation in the mRNA expression of SOX9 and Col2a1 (**Supplementary Figure 4g, h**). For ER stress pathway we detected the reduction in IRE1α expressionand upregulated CHOP expression in the SgDDRGK1 pellet compared with SgNC pellet in immunofluorescence test (Figure 6E **and Supplementary Figure 4g**), causing disruption in the chondrogenesis process. Using TUNEL staining to evaluate the apoptotic status of the pellet culture of SgNC and SgDDRGK cells, we found that the number of TUNEL-positive cells was significantly increased in the SgDDRGK1 pellet, suggesting that the loss of DDRGK1 increased the apoptosis rate in SgDDRGK1 cells and impaired its chondrogenesis ability (Figure 6B,D).

Discussion

In our study, we first divided the ATDC5 chondrocytes into the SgDDRGK1 and SgNC groups *in vitro* using the CRISPR/cas9 technology. It was found that DDRGK1 knockout significantly inhibited their differentiation ability whilst inducing apoptosis downstream of excessive ER stress. The function of IRE1α is closely associated with DDRGK1 and regulates ER stress[31]. DDRGK1 knockout was found to

decrease UFMylation, resulting in the increased ubiquitylation-mediated degradation of IRE1α. This form of IRE1α destruction caused an imbalance in the homeostasis of ER physiology, which activated the PERK/CHOP pathway and upregulated the Bax/Bcl-2 ratio, leading to the cleavage of caspase 3 and PARP and apoptosis (Figure 7).

Growth and development of tissues involve a variety of regulators that coordinate and control specific developmental pathways[30]. For example, runt-related transcription factor 1, myoblast determination protein 1 and T-cell acute leukemia protein 1 serve as the main transcription factors that regulate the differentiation of primitive osteoblasts, skeletal muscle and red blood cells, respectively[32–34]. In addition, there is accumulating evidence that SOX9 is a unique, key transcription factor underlying chondrogenesis[7, 35]. In addition, it has also been found to regulate the development of other systems, including gonads, glia and the heart valve[35–37]. As such, various diseases have also been associated with dysregulated SOX9. Insufficient haplotype of SOX9 can lead to myelodysplasia [38, 39], whereas decreased expression of SOX9 can cause SEMD[40]. SEMD is a form of neonatal achondroplasia that was recently revealed to be canonically caused by the relationship between DDRGK1 and SOX9[7]. In the present study, we believe that DDRGK1 serves a different but important role: Stabilizing proteins on the ER membrane.

The ER is a key organelle that is involved in a variety of processes. Disturbances in the ER can activate the UPR, which can in turn either mediate cell survival if ER homeostasis is gradually restored or trigger apoptosis if the UPR becomes chronic or excessive[17, 41, 42]. There are mainly three sensory receptors on the surface of the ER, namely IRE1α, PERK and activating transcription factor 6[43–45]. During the early stages of the UPR, IRE1α splices the mRNA of the transcription factor X-box binding protein 1 to induce the transcription of ER quality control components like XBP1 to restore endoplasmic reticulum homeostasis[28, 46] and promote cell survival. If IRE1α fails to maintain homeostasis, then apoptosis becomes activated through c-Jun N-terminal kinase signaling[47]. PERK directly phosphorylates the subunit of eukaryotic initiation factor 2, which selectively translates and activating transcription factor 4 to upregulate the expression of a multitude of UPR target genes, including those involved in ER stress-mediated apoptosis, such as C/EBP homologous protein (CHOP)[48].

During this process, DDRGK1, which is an ER transmembrane protein and a key component of the UFM1 system, is also responsible for modifying IRE1α. In the present study, we found one of these post-translational modifications to be UFMylation, which consists of the dynamic E1-E2-E3 cascade of reactions mediated by ubiquitin-like modifier activating enzyme 5, UFL1, UFC1 and DDRGK1[49]. DDRGK1 itself can not only serve as a substrate of UFMylation but has also been shown to serve as a cofactor in the UFMylation of cyclin-dependent kinase-5 regulatory subunit associated protein 3, p53 and guanine nucleotide-binding protein subunit β-like protein[11, 50, 51]. In addition, DDRGK1 has been reported to facilitate protein UFMylation to maintain their stability in a number of diseases, including uterine endometrioid carcinoma, neurodegenerative disease and developmental defect diseases[12, 52, 53]. A recent study showed that UFM1 and UFC1 are important for the development of the brain during embryogenesis in humans[54]. In the present study a connection between the DDRGK1 with ER was

revealed, where DDRGK1 facilitated the UFMylation of IRE1α to maintain its presence and activity in ATDC5 chondrocytes. Previous studie have shown that DDRGK1 regulated the stability of IRE1α in several types of cancer cells like MCF7 and HepG2 cells[16]. These observations suggest that deletion of DDRGK1 leads to the reduced UFMylation of IRE1α, which was found in renal tumor cells, where the loss of UFMylation increased the ubiquitylation and degradation of p53[9]. In ATDC5 chondrocytes, DDRGK1 knockout also increased the ubiquitylation-mediated degradation of IRE1α, followed by UPR activation and cell apoptosis.

Apoptosis is a form of programmed cell death that plays key roles in pathological conditions, such as microbial infection, autoimmune diseases and even coronavirus infection[55–57]. Although it can also function as a negative feedback mechanism during tissue development and regeneration[58], dysregulation of apoptosis can result in various types of complex abnormalities[59]. Together with pyroptosis and necrosis, apoptosis is an end-point event of cell death[60]. However, the process of apoptosis itself is a two-sided event. In tumor cells like hepatic carcinoma cells and breast cancer cells, apoptosis may be beneficial[61, 62]. By contrast, for normal cells it is necessary to avoid apoptosis where possible[63]. Apoptosis involves the continuous activation of a series of cysteine proteases called Caspases[64]. Caspases are present in the cytoplasm of the majority of cells mainly in the inactive pro-caspase form[65]. Under certain conditions, caspases can activate itself through autocatalytic cleavage, where it can then cleave and activate other caspases to activate the self-amplifying cascade[66]. Promoter caspases, such as caspase-9, cleave and activate downstream effector caspases, such as caspase-3, which in turn cleaves a number of cellular proteins, including the cytoskeletal protein PARP[67]. In mammalian cells, mitochondria serve an important role in apoptosis and caspase activation[68].

Conclusion

In conclusion, in the present study we mainly focused on the relationship among apoptosis, cartilage differentiation and ER stress. By applying DDRGK1 knockout ATDC5 chondrocytes, a DDRGK1/UFMylation system was revealed and characterized, where the degradation of IRE1α and the ensuing CHOP/apoptosis activation but not the activation of PANoptosis [pyroptosis, apoptosis and necrosis, we only detected increased Bax, decreased Bcl-2, cleaved caspase 3 and PARP in ATDC5 chondrocytes. As for the pyroptosis marker GSDMD and the necrosis marker RIP, there was no evident effects (Figure 1G **and Supplementary Figure 1a**)]. This process may at least in part underlie the phenomenon of growth retardation that occurs during SEMD pathogenesis, which includes abnormal spinal development[69]. It is hoped that data in this study can provide a novel gene target for future SEMD treatment. For patients clinically suffering from spine epiphyseal dysplasia, the DDRGK1 gene should be focused upon as a potential target and from the perspective of gene treatment, DDRGK1-targeted gene therapy may be considered as a novel approach in the future.

Abbreviations

SEMD: Spondyloepiphyseal dysplasia; UPR: unfolded protein response; ER: endoplasmic reticulum membrane; UFBP1: UFM1 binding protein 1 with PCI domain; ERα: estrogen receptor α; ASC1: activating signal cointegrator 1; SOFG: safranin o-fast green; IOD: integral optical density; BAX: BCL2 associated X, apoptosis regulator; BCL2: B cell leukemia/lymphoma 2 apoptosis regulator; PARP: Poly-(ADP-ribose) polymerase; GSDMD: gasdermin D; RIP: regulation of phenobarbitol-inducible P450; ECM: extracellular matrix; Col2a1: collagen type II alpha 1 chain; CHOP: C/EBP homologous protein; CHX: Cycloheximide; Chlq: chloroquine; WCL: whole cell lysate; Tg: Thapsigargin; BIP: ER luminal binding protein precursor; PERK: PKR-like endoplasmic reticulum kinase; SOX9: SRY (sex determining region Y)-box 9; RUNX2: runt related transcription factor 2; MYOD: myogenic differentiation; TAL1: T cell acute lymphocytic leukemia 1; CMD: myelodysplasia; ATF6: activating transcription factor 6; XBP1: X-box binding protein 1; JNK: mitogen-activated protein kinase 9; eIF2a: eukaryotic initiation factor 2; ATF4: activates transcription factor 4; UBA5: ubiquitin like modifier activating enzyme 5; UFL1: UFM1 specific ligase 1; UFC1: ubiquitin-fold modifier conjugating enzyme 1; CDK5RAP3: CDK5 regulatory subunit associated protein 3; UFM1: ubiquitin fold modifier 1

Declarations

Ethical Approval and Consent to participate

Not applicable.

Consent for publication

Not applicable.

Availability of supporting data

All data included in this study are available upon request by contact with the corresponding author

Competing interests

The authors declare that the research was conducted in the absence of any commercial or financial relationships that could be construed as a potential conflict of interest.

Funding

The present study was supported by grants from The National Natural Science Foundation of China (grant nos. 82130073, 81871790, 81572768 and 81972136).

Author contributions

JZ, AQ and HM designed the research and guided all the experiments. XY, YX and TJZ performed the experiments, organized the data and wrote the manuscript. HM and HJT performed statistical analysis and reviewed the manuscript critically for important intellectual content. XFC and YC analyzed the

data, confirmed the authenticity of all the raw data and helped to write the manuscript. All authors read and approved the final manuscript.

Acknowledgements

The authors would like to thank The Flow Cytometry Lab of Bioimaging Facility (Shanghai Institute of Precision Medicine, Shanghai, China) for providing the BD LSRFortessa machine and guidance of operation from Professor Shuai Li.

Authors' information

Affiliations

Shanghai Key Laboratory of Orthopedic Implants, Department of Orthopedics, Ninth People's Hospital, Shanghai Jiaotong University School of Medicine, 639 Zhizaoju Road, Shanghai, 200011, P. R. China

Xiao Yang, Tangjun Zhou, Haijun Tian, Xiaofei Cheng, Yu Cao, Hui Ma, An Qin, Jie Zhao

Institute of Precision Medicine, The Ninth People's Hospital, Shanghai Jiao Tong University School of Medicine, Shanghai 200125, China

Ying Xia, Yu Cao

References

1. Horton WA, Hall JG, Hecht JT: **Achondroplasia**. *Lancet* 2007, **370**(9582):162-172.
2. Spranger J, Winterpacht A, Zabel B: **The type II collagenopathies: a spectrum of chondrodysplasias**. *Eur J Pediatr* 1994, **153**(2):56-65.
3. Kuivaniemi H, Tromp G, Prockop DJ: **Mutations in fibrillar collagens (types I, II, III, and XI), fibril-associated collagen (type IX), and network-forming collagen (type X) cause a spectrum of diseases of bone, cartilage, and blood vessels**. *Hum Mutat* 1997, **9**(4):300-315.
4. Wirth T: **[Spondyloepiphyseal and metaphyseal dysplasia]**. *Orthopade* 2008, **37**(1).
5. Cormier-Daire V: **Spondylo-epi-metaphyseal dysplasia**. *Best Pract Res Clin Rheumatol* 2008, **22**(1):33-44.
6. Shohat M, Lachman R, Carmi R, Bar Ziv J, Rimoin D: **New form of spondyloepimetaphyseal dysplasia (SEMD) in Jewish family of Iraqi origin**. *Am J Med Genet* 1993, **46**(4):358-362.
7. Egunsola AT, Bae Y, Jiang M-M, Liu DS, Chen-Evenson Y, Bertin T, Chen S, Lu JT, Nevarez L, Magal N *et al*: **Loss of DDRGK1 modulates SOX9 ubiquitination in spondyloepimetaphyseal dysplasia**. *J Clin Invest* 2017, **127**(4):1475-1484.
8. Liang JR, Lingeman E, Luong T, Ahmed S, Muhar M, Nguyen T, Olzmann JA, Corn JE: **A Genome-wide ER-phagy Screen Highlights Key Roles of Mitochondrial Metabolism and ER-Resident UFMylation**. *Cell* 2020, **180**(6).

9. Liu J, Guan D, Dong M, Yang J, Wei H, Liang Q, Song L, Xu L, Bai J, Liu C *et al*: **UFMylation maintains tumour suppressor p53 stability by antagonizing its ubiquitination**. *Nat Cell Biol* 2020, **22**(9):1056-1063.
10. Cai Y, Pi W, Sivaprakasam S, Zhu X, Zhang M, Chen J, Makala L, Lu C, Wu J, Teng Y *et al*: **UFBP1, a Key Component of the Ufm1 Conjugation System, Is Essential for Ufmylation-Mediated Regulation of Erythroid Development**. *PLoS Genet* 2015, **11**(11):e1005643.
11. Gerakis Y, Quintero M, Li H, Hetz C: **The UFMylation System in Proteostasis and Beyond**. *Trends Cell Biol* 2019, **29**(12):974-986.
12. Wang L, Xu Y, Rogers H, Saidi L, Noguchi CT, Li H, Yewdell JW, Guydosh NR, Ye Y: **UFMylation of RPL26 links translocation-associated quality control to endoplasmic reticulum protein homeostasis**. *Cell Res* 2020, **30**(1).
13. Xi P, Ding D, Zhou J, Wang M, Cong Y-S: **DDRGK1 regulates NF-κB activity by modulating IκBα stability**. *PLoS ONE* 2013, **8**(5):e64231.
14. Zhu H, Bhatt B, Sivaprakasam S, Cai Y, Liu S, Kodeboyina SK, Patel N, Savage NM, Sharma A, Kaufman RJ *et al*: **Ufbp1 promotes plasma cell development and ER expansion by modulating distinct branches of UPR**. *Nature communications* 2019, **10**(1):1084.
15. Yoo HM, Kang SH, Kim JY, Lee JE, Seong MW, Lee SW, Ka SH, Sou Y-S, Komatsu M, Tanaka K *et al*: **Modification of ASC1 by UFM1 is crucial for ERα transactivation and breast cancer development**. *Mol Cell* 2014, **56**(2):261-274.
16. Liu J, Wang Y, Song L, Zeng L, Yi W, Liu T, Chen H, Wang M, Ju Z, Cong Y-S: **A critical role of DDRGK1 in endoplasmic reticulum homoeostasis via regulation of IRE1α stability**. *Nature Communications* 2017, **8**(1):14186.
17. Hetz C: **The unfolded protein response: controlling cell fate decisions under ER stress and beyond**. *Nat Rev Mol Cell Biol* 2012, **13**(2).
18. Zhang K, Wang S, Malhotra J, Hassler JR, Back SH, Wang G, Chang L, Xu W, Miao H, Leonardi R *et al*: **The unfolded protein response transducer IRE1α prevents ER stress-induced hepatic steatosis**. *EMBO J* 2011, **30**(7):1357-1375.
19. Cubillos-Ruiz JR, Bettigole SE, Glimcher LH: **Tumorigenic and Immunosuppressive Effects of Endoplasmic Reticulum Stress in Cancer**. *Cell* 2017, **168**(4):692-706.
20. Hetz C, Saxena S: **ER stress and the unfolded protein response in neurodegeneration**. *Nat Rev Neurol* 2017, **13**(8):477-491.
21. Reverendo M, Mendes A, Argüello RJ, Gatti E, Pierre P: **At the crossway of ER-stress and proinflammatory responses**. *FEBS J* 2019, **286**(2):297-310.
22. Walter P, Ron D: **The unfolded protein response: from stress pathway to homeostatic regulation**. *Science* 2011, **334**(6059):1081-1086.
23. Merksamer PI, Papa FR: **The UPR and cell fate at a glance**. *J Cell Sci* 2010, **123**(Pt 7):1003-1006.

24. Livak KJ, Schmittgen TD: **Analysis of relative gene expression data using real-time quantitative PCR and the 2(-Delta Delta C(T)) Method**. *Methods* 2001, **25**(4):402-408.
25. Wu B, Durisin EK, Decker JT, Ural EE, Shea LD, Coleman RM: **Phosphate regulates chondrogenesis in a biphasic and maturation-dependent manner**. *Differentiation* 2017, **95**:54-62.
26. Shi J-W, Zhang T-T, Liu W, Yang J, Lin X-L, Jia J-S, Shen H-F, Wang S-C, Li J, Zhao W-T *et al*: **Direct conversion of pig fibroblasts to chondrocyte-like cells by c-Myc**. *Cell Death Discov* 2019, **5**:55.
27. Hwang J, Qi L: **Quality Control in the Endoplasmic Reticulum: Crosstalk between ERAD and UPR pathways**. *Trends Biochem Sci* 2018, **43**(8):593-605.
28. Lin JH, Li H, Yasumura D, Cohen HR, Zhang C, Panning B, Shokat KM, Lavail MM, Walter P: **IRE1 signaling affects cell fate during the unfolded protein response**. *Science* 2007, **318**(5852):944-949.
29. Luo Y, Sinkeviciute D, He Y, Karsdal M, Henrotin Y, Mobasheri A, Önnerfjord P, Bay-Jensen A: **The minor collagens in articular cartilage**. *Protein Cell* 2017, **8**(8):560-572.
30. Song H, Park K-H: **Regulation and function of SOX9 during cartilage development and regeneration**. *Semin Cancer Biol* 2020, **67**(Pt 1):12-23.
31. Liu J, Wang Y, Song L, Zeng L, Yi W, Liu T, Chen H, Wang M, Ju Z, Cong Y-S: **A critical role of DDRGK1 in endoplasmic reticulum homoeostasis via regulation of IRE1α stability**. *Nat Commun* 2017, **8**:14186.
32. Komori T: **Runx2, a multifunctional transcription factor in skeletal development**. *J Cell Biochem* 2002, **87**(1):1-8.
33. Weintraub H, Tapscott SJ, Davis RL, Thayer MJ, Adam MA, Lassar AB, Miller AD: **Activation of muscle-specific genes in pigment, nerve, fat, liver, and fibroblast cell lines by forced expression of MyoD**. *Proc Natl Acad Sci USA* 1989, **86**(14):5434-5438.
34. Porcher C, Swat W, Rockwell K, Fujiwara Y, Alt FW, Orkin SH: **The T cell leukemia oncoprotein SCL/tal-1 is essential for development of all hematopoietic lineages**. *Cell* 1996, **86**(1):47-57.
35. Akiyama H, Chaboissier M-C, Behringer RR, Rowitch DH, Schedl A, Epstein JA, de Crombrugghe B: **Essential role of Sox9 in the pathway that controls formation of cardiac valves and septa**. *Proceedings of the National Academy of Sciences of the United States of America* 2004, **101**(17):6502-6507.
36. Jo A, Denduluri S, Zhang B, Wang Z, Yin L, Yan Z, Kang R, Shi LL, Mok J, Lee MJ *et al*: **The versatile functions of Sox9 in development, stem cells, and human diseases**. *Genes Dis* 2014, **1**(2):149-161.
37. Kang P, Lee HK, Glasgow SM, Finley M, Donti T, Gaber ZB, Graham BH, Foster AE, Novitch BG, Gronostajski RM *et al*: **Sox9 and NFIA coordinate a transcriptional regulatory cascade during the initiation of gliogenesis**. *Neuron* 2012, **74**(1):79-94.
38. Kwok C, Weller PA, Guioli S, Foster JW, Mansour S, Zuffardi O, Punnett HH, Dominguez-Steglich MA, Brook JD, Young ID: **Mutations in SOX9, the gene responsible for Campomelic dysplasia and autosomal sex reversal**. *Am J Hum Genet* 1995, **57**(5):1028-1036.

39. Wang H, McKnight NC, Zhang T, Lu ML, Balk SP, Yuan X: **SOX9 is expressed in normal prostate basal cells and regulates androgen receptor expression in prostate cancer cells**. *Cancer Res* 2007, **67**(2):528-536.
40. Mansour S, Offiah AC, McDowall S, Sim P, Tolmie J, Hall C: **The phenotype of survivors of campomelic dysplasia**. *J Med Genet* 2002, **39**(8):597-602.
41. Brown MK, Naidoo N: **The endoplasmic reticulum stress response in aging and age-related diseases**. *Front Physiol* 2012, **3**:263.
42. Xu C, Bailly-Maitre B, Reed JC: **Endoplasmic reticulum stress: cell life and death decisions**. *J Clin Invest* 2005, **115**(10):2656-2664.
43. Rutkowski DT, Kaufman RJ: **A trip to the ER: coping with stress**. *Trends Cell Biol* 2004, **14**(1):20-28.
44. Tabas I, Ron D: **Integrating the mechanisms of apoptosis induced by endoplasmic reticulum stress**. *Nat Cell Biol* 2011, **13**(3):184-190.
45. Jing G, Wang JJ, Zhang SX: **ER stress and apoptosis: a new mechanism for retinal cell death**. *Exp Diabetes Res* 2012, **2012**:589589.
46. Chen L, Xu S, Liu L, Wen X, Xu Y, Chen J, Teng J: **Cab45S inhibits the ER stress-induced IRE1-JNK pathway and apoptosis via GRP78/BiP**. *Cell Death Dis* 2014, **5**:e1219.
47. Li Y, Jiang W, Niu Q, Sun Y, Meng C, Tan L, Song C, Qiu X, Liao Y, Ding C: **eIF2α-CHOP-BCl-2/JNK and IRE1α-XBP1/JNK signaling promote apoptosis and inflammation and support the proliferation of Newcastle disease virus**. *Cell Death Dis* 2019, **10**(12):891.
48. Urano F, Wang X, Bertolotti A, Zhang Y, Chung P, Harding HP, Ron D: **Coupling of stress in the ER to activation of JNK protein kinases by transmembrane protein kinase IRE1**. *Science* 2000, **287**(5453):664-666.
49. Bacik J-P, Walker JR, Ali M, Schimmer AD, Dhe-Paganon S: **Crystal structure of the human ubiquitin-activating enzyme 5 (UBA5) bound to ATP: mechanistic insights into a minimalistic E1 enzyme**. *J Biol Chem* 2010, **285**(26):20273-20280.
50. Jiang H, Wu J, He C, Yang W, Li H: **Tumor suppressor protein C53 antagonizes checkpoint kinases to promote cyclin-dependent kinase 1 activation**. *Cell Res* 2009, **19**(4):458-468.
51. Kwon J, Cho HJ, Han SH, No JG, Kwon JY, Kim H: **A novel LZAP-binding protein, NLBP, inhibits cell invasion**. *J Biol Chem* 2010, **285**(16):12232-12240.
52. Wang Z, Gong Y, Peng B, Shi R, Fan D, Zhao H, Zhu M, Zhang H, Lou Z, Zhou J *et al*: **MRE11 UFMylation promotes ATM activation**. *Nucleic Acids Res* 2019, **47**(8):4124-4135.
53. Qin B, Yu J, Nowsheen S, Wang M, Tu X, Liu T, Li H, Wang L, Lou Z: **UFL1 promotes histone H4 ufmylation and ATM activation**. *Nature communications* 2019, **10**(1):1242.
54. Nahorski MS, Maddirevula S, Ishimura R, Alsahli S, Brady AF, Begemann A, Mizushima T, Guzmán-Vega FJ, Obata M, Ichimura Y *et al*: **Biallelic UFM1 and UFC1 mutations expand the essential role of ufmylation in brain development**. *Brain* 2018, **141**(7):1934-1945.

55. Place DE, Lee S, Kanneganti T-D: **PANoptosis in microbial infection**. *Curr Opin Microbiol* 2021, **59**:42-49.
56. Place DE, Kanneganti T-D: **The innate immune system and cell death in autoinflammatory and autoimmune disease**. *Curr Opin Immunol* 2020, **67**.
57. Lee S, Channappanavar R, Kanneganti T-D: **Coronaviruses: Innate Immunity, Inflammasome Activation, Inflammatory Cell Death, and Cytokines**. *Trends Immunol* 2020, **41**(12):1083-1099.
58. Nijhawan D, Honarpour N, Wang X: **Apoptosis in neural development and disease**. *Annu Rev Neurosci* 2000, **23**:73-87.
59. Tower J: **Programmed cell death in aging**. *Ageing Res Rev* 2015, **23**(Pt A).
60. Majno G, Joris I: **Apoptosis, oncosis, and necrosis. An overview of cell death**. *Am J Pathol* 1995, **146**(1).
61. Wang C, Vegna S, Jin H, Benedict B, Lieftink C, Ramirez C, de Oliveira RL, Morris B, Gadiot J, Wang W *et al*: **Inducing and exploiting vulnerabilities for the treatment of liver cancer**. *Nature* 2019, **574**(7777):268-272.
62. Sinha D, Sarkar N, Biswas J, Bishayee A: **Resveratrol for breast cancer prevention and therapy: Preclinical evidence and molecular mechanisms**. *Semin Cancer Biol* 2016, **40-41**:209-232.
63. Maiuri MC, Zalckvar E, Kimchi A, Kroemer G: **Self-eating and self-killing: crosstalk between autophagy and apoptosis**. *Nat Rev Mol Cell Biol* 2007, **8**(9):741-752.
64. Shalini S, Dorstyn L, Dawar S, Kumar S: **Old, new and emerging functions of caspases**. *Cell Death Differ* 2015, **22**(4):526-539.
65. Carmona-Gutierrez D, Fröhlich KU, Kroemer G, Madeo F: **Metacaspases are caspases. Doubt no more**. *Cell Death Differ* 2010, **17**(3):377-378.
66. Chihara T, Kitabayashi A, Morimoto M, Takeuchi K-i, Masuyama K, Tonoki A, Davis RL, Wang JW, Miura M: **Caspase inhibition in select olfactory neurons restores innate attraction behavior in aged Drosophila**. *PLoS Genet* 2014, **10**(6):e1004437.
67. Cohausz O, Althaus FR: **Role of PARP-1 and PARP-2 in the expression of apoptosis-regulating genes in HeLa cells**. *Cell Biol Toxicol* 2009, **25**(4):379-391.
68. Delavallée L, Cabon L, Galán-Malo P, Lorenzo HK, Susin SA: **AIF-mediated caspase-independent necroptosis: a new chance for targeted therapeutics**. *IUBMB Life* 2011, **63**(4):221-232.
69. Kennedy AM, Inada M, Krane SM, Christie PT, Harding B, López-Otín C, Sánchez LM, Pannett AAJ, Dearlove A, Hartley C *et al*: **MMP13 mutation causes spondyloepimetaphyseal dysplasia, Missouri type (SEMD(MO)**. *J Clin Invest* 2005, **115**(10):2832-2842.

Figures

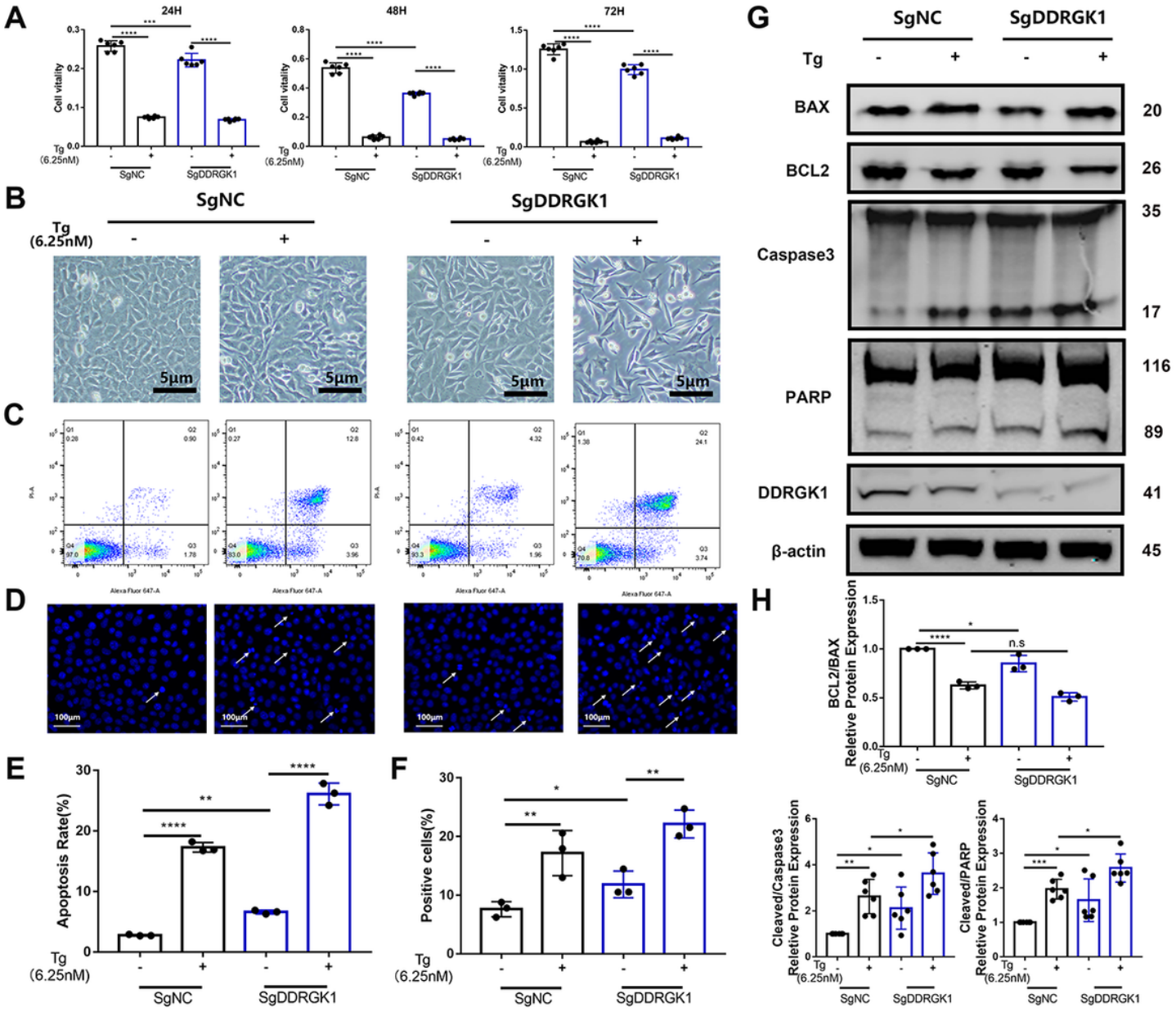

Figure 1

Loss of DDRGK1 in ATDC5 cells led to apoptosis which deteriorated with ER stress. (A) Cell viability of SgNC and SgDDRGK1 ATDC5 chondrocytes with or without thapsigargin (6.25 nM) treatment for 24, 48 and 72 h. (B) Cell morphology of SgNC and SgDDRGK1 ATDC5 chondrocytes with or without thapsigargin (6.25 nM) treatment. (C) Flow cytometry of SgNC and SgDDRGK1 ATDC5 chondrocytes 24 h after treatment with or without thapsigargin (6.25 nM). (D) Hoechst staining of SgNC and SgDDRGK1 ATDC5 chondrocytes after treatment with or without Tg (6.25nM) for 24 h. Karyopyknosis of the cell nucleus was observed using DAPI staining. (E) Quantification of the apoptosis rate (Q2 + Q3) using flow cytometry of cells in (C). (F) Quantification of cells positive for karyopyknosis in the nucleus with respect to the total number of nuclei using Hoechst and DAPI staining of cells in (D). (G) Western blot analysis of Bax, Bcl2, cleaved and total caspase 3, cleaved and total PARP, DDRGK1 and β-actin expression in SgNC and SgDDRGK1 ATDC5 chondrocytes. (H) Quantification of the gray values as the ratio of Bax/Bcl2,

cleaved/total caspase 3 and cleaved/total PARP in SgNC and SgDDRGK1 ATDC5 chondrocytes. All data are presented as the mean ± SD from three or more experiments. *P < 0.05, **P < 0.01, ***P < 0.001 and ****P < 0.0001.

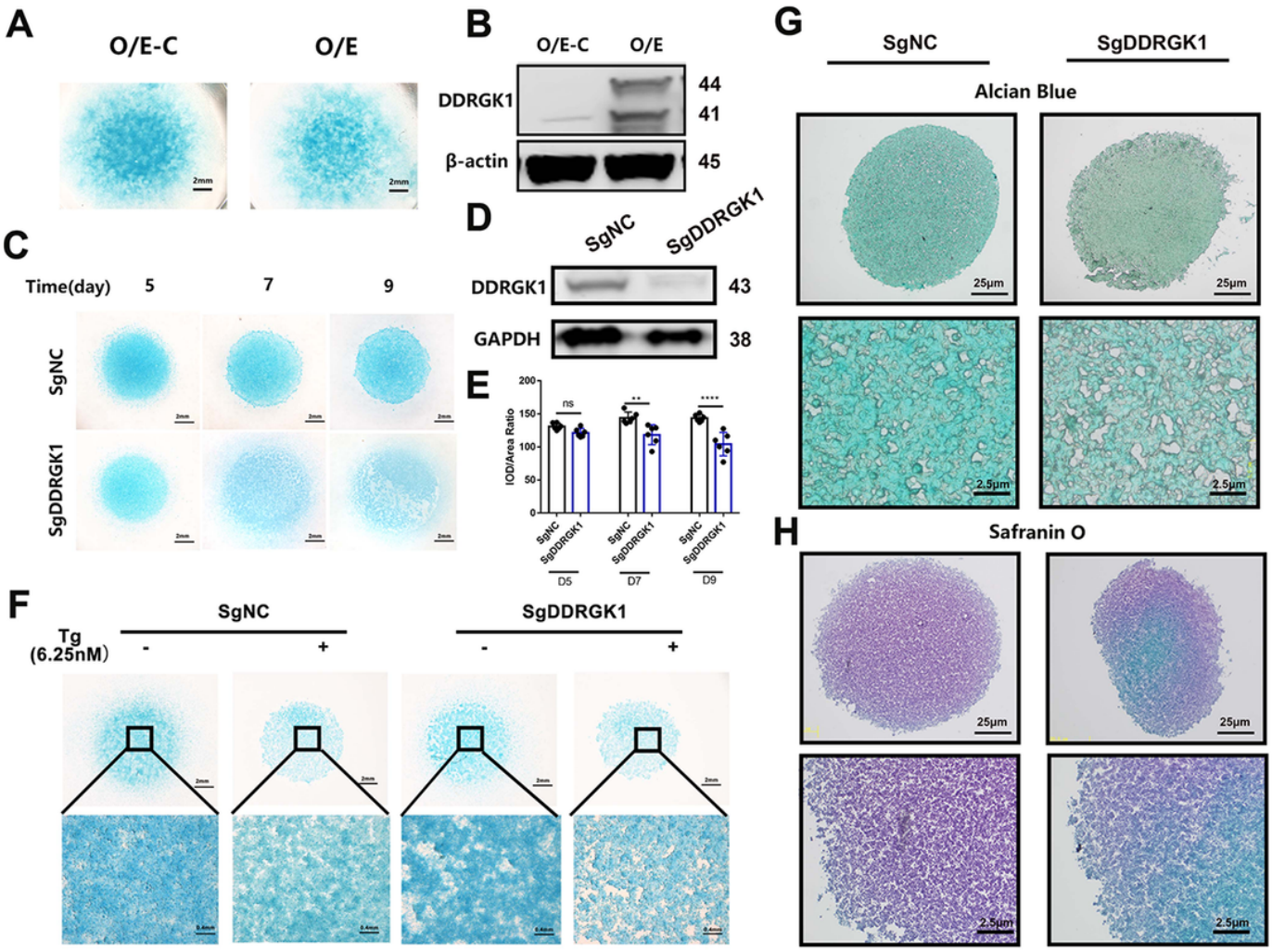

Figure 2

Loss of DDRGK1 expression impaired ATDC cell chondrogenesis but DDRGK1 overexpression had no effect on this ability in vitro. (A) Alcian blue stain of O/E-C and O/E ATDC5 chondrocytes after 9 days of high-density culture in DMEM/F12 medium containing 10 ng/ml ITS.. (B) Western blot analysis of the DDRGK1 protein on O/E-C and O/E ATDC5 chondrocytes used β-actin as reference. (C) Alcian blue stain of SgNC and SgDDRGK1 ATDC5 chondrocytes 5, 7 and 9 days after high-density culture in chondrogenesis medium. (D) Western blot analysis of the DDRGK1 protein on SgNC and SgDDRGK1 ATDC5 chondrocytes used β-actin as reference. (E) Quantification of the IOD/Area ratio of Alcian blue staining of cells shown in (C) using the Image Pro Plus 6.0 software. (F) Alcian blue stain of SgNC and SgDDRGK1 ATDC5 chondrocytes after 9 days of high-density culture in chondrogenesis medium with or without thapsigargin. (G) Alcian blue stain of SgNC and SgDDRGK1 ATDC5 chondrocytes 21 days after pellet culture in chondrogenesis medium. (H) Safranin O-Fast Green staining of SgNC and SgDDRGK1

ATDC5 chondrocytes 21 days after pellet culture in chondrogenesis medium. All data are presented as the mean ± SD. * P < 0.05, **P < 0.01, ***P < 0.001 and ****P < 0.0001.

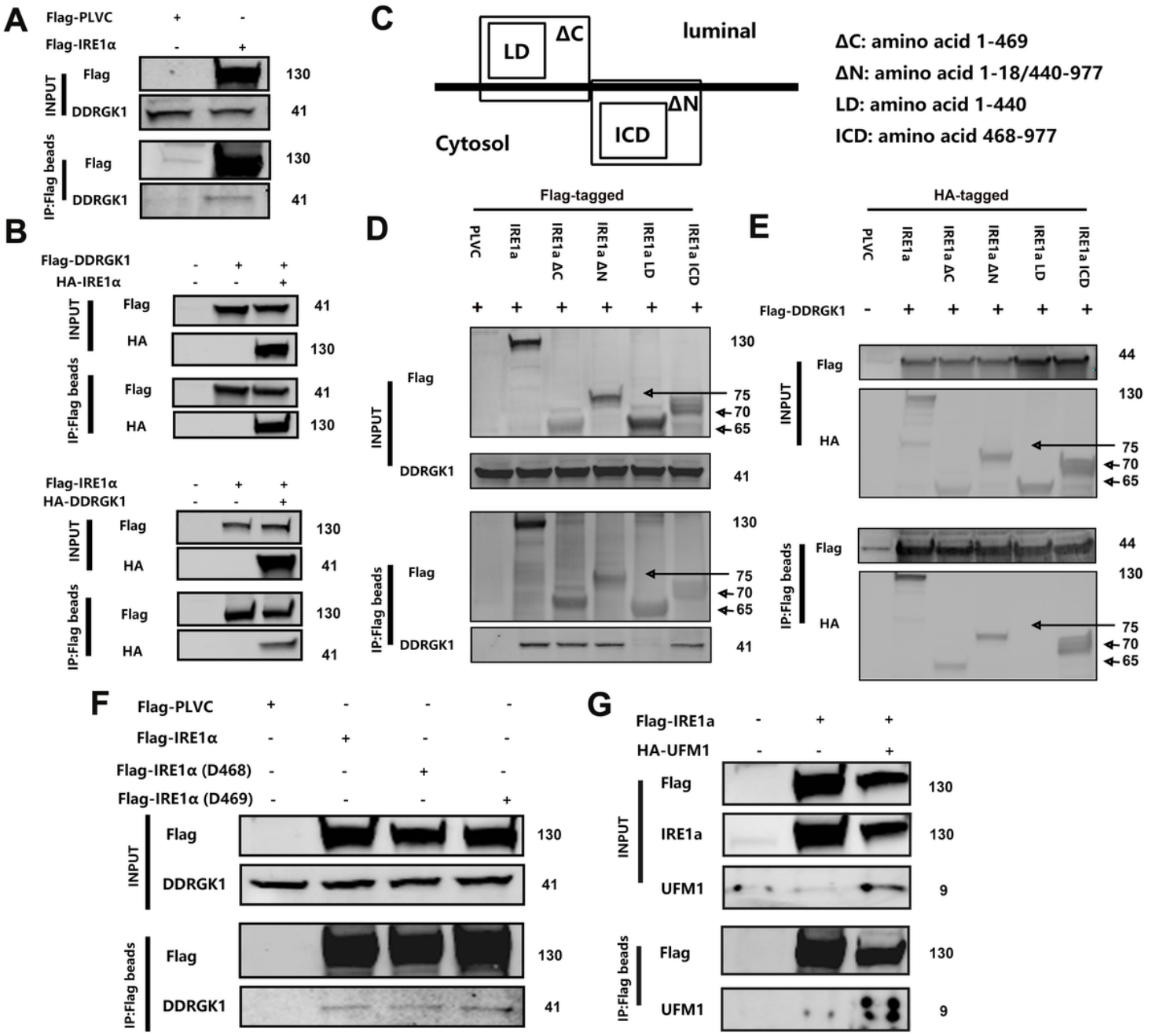

Figure 3

DDRGK1 interacts with IRE1α on multiple sites way in vitro. (A) Co-immunoprecipitation analysis of the possible interaction between Flag-IRE1α and DDRGK1 using Flag-tagged beads in 293T cells. (B) Co-immunoprecipitation analysis of the possible interaction between Flag-DDRGK1 and HA-IRE1α, and between Flag-IRE1α and HA-DDRGK1 using Flag-tagged beads in 293T cells. (C) Graphical illustration of HA (Flag)-IRE1α ΔC, HA (Flag)-IRE1α ΔN, HA (Flag)-IRE1α LD and HA (Flag)-IRE1α ICD. (D) Co-immunoprecipitation analysis of the possible interaction between Flag-IRE1α, Flag-IRE1α ΔC, Flag-IRE1α ΔN, Flag-IRE1α LD or Flag-IRE1α ICD and DDRGK1 using Flag-tagged beads in 293T cells. (E) Co-

immunoprecipitation analysis of the possible interaction between Flag-DDRGK1 and HA-IRE1α, HA-IRE1α ΔC, HA-IRE1α ΔN, HA-IRE1α LD or HA-IRE1α ICD using Flag-tagged beads in 293T cells. (F) Co-immunoprecipitation analysis of the possible interaction between Flag-IRE1α, Flag-IRE1α D468 or Flag-IRE1α D469 and DDRGK1 using Flag-tagged beads in 293T cells. (G) Co-immunoprecipitation analysis of the possible interaction between Flag-IRE1α and HA-UFM1 using Flag-tagged beads in 293T cells.

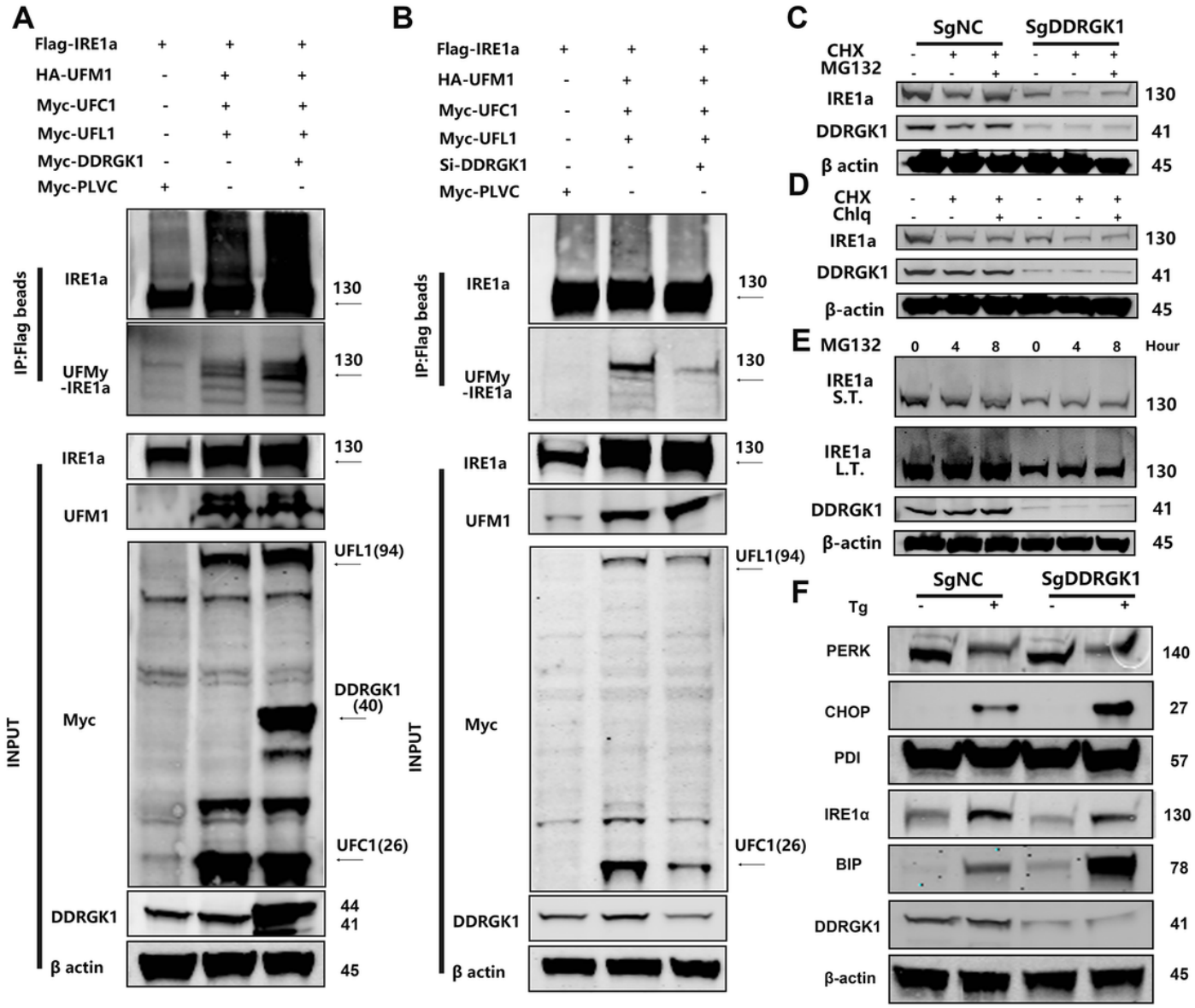

Figure 4

Loss of DDRGK1 impairs the UFMylation of IRE1α, leading to its degradation and subsequently promote ER stress in vitro. (A) UFMylation analysis of Flag-IRE1α using Flag-PLVC, HA-UFM1, Myc-DDRGK1, Myc-UFL1 and Myc-UFC1 plasmids in 293T cells pulled down by Flag-tagged beads. (B) UFMylation analysis of Flag-IRE1α using Flag-PLVC, HA-UFM1, si-DDRGK1, Myc-UFL1 and Myc-UFC1 plasmids in 293T cells pulled down by Flag-tagged beads. (C) Western blot analysis of IRE1α and DDRGK1 using β-actin as the loading control in SgNC and SgDDRGK1 ATDC5 chondrocytes treated with cycloheximide (50 nM) and MG132 (10 μM). (D) Western blot analysis of IRE1α and DDRGK1 using β-actin as the loading control in

SgNC and SgDDRGK1 ATDC5 chondrocytes treated with cycloheximide (50 nM) and chloroquine (25 nM). (E) Western blot analysis of IRE1α and DDRGK1 using β-actin as the loading control in SgNC and SgDDRGK1 ATDC5 chondrocytes treated with MG132 (10 μM) for 0, 4 and 8 h. L.T. Long exposure time. S.T. Short exposure time. (F) Western blot analysis of PERK, CHOP, PDI, IRE1α, BiP and DDRGK1 using β-actin as the loading control in SgNC and SgDDRGK1 ATDC5 chondrocytes treated with thapsigargin for 24 h.

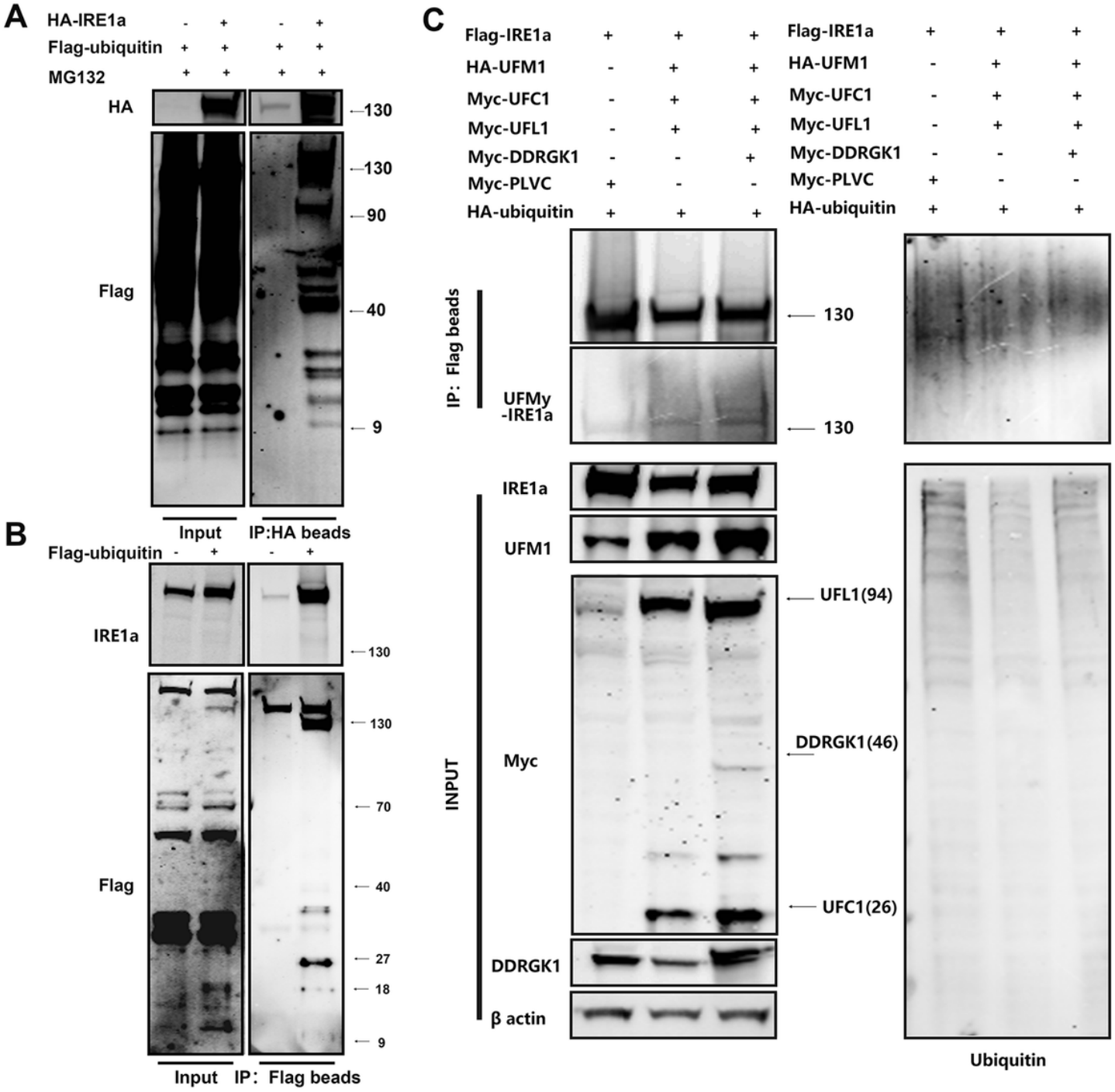

Figure 5

Ubiquitylation of IRE1α led to degradation whereas UFMylation antagonizes this in vitro. (A) Ubiquitylation analysis of IRE1α in 293T cells treated with MG132 (10 μM) using HA-IRE1α and Flag-

ubiquitin plasmids with HA-tagged beads. (B) Ubiquitylation analysis of intrinsic IRE1α using the Flag-Ubiquitin plasmid and Flag-tagged beads in 293T cells. (C) UFMylation analysis of Flag-IRE1α using the Flag-PLVC, HA-UFM1, Myc-DDRGK1, Myc-UFL1, Myc-UFC1 and HA-ubiquitin plasmids in 293T cells.

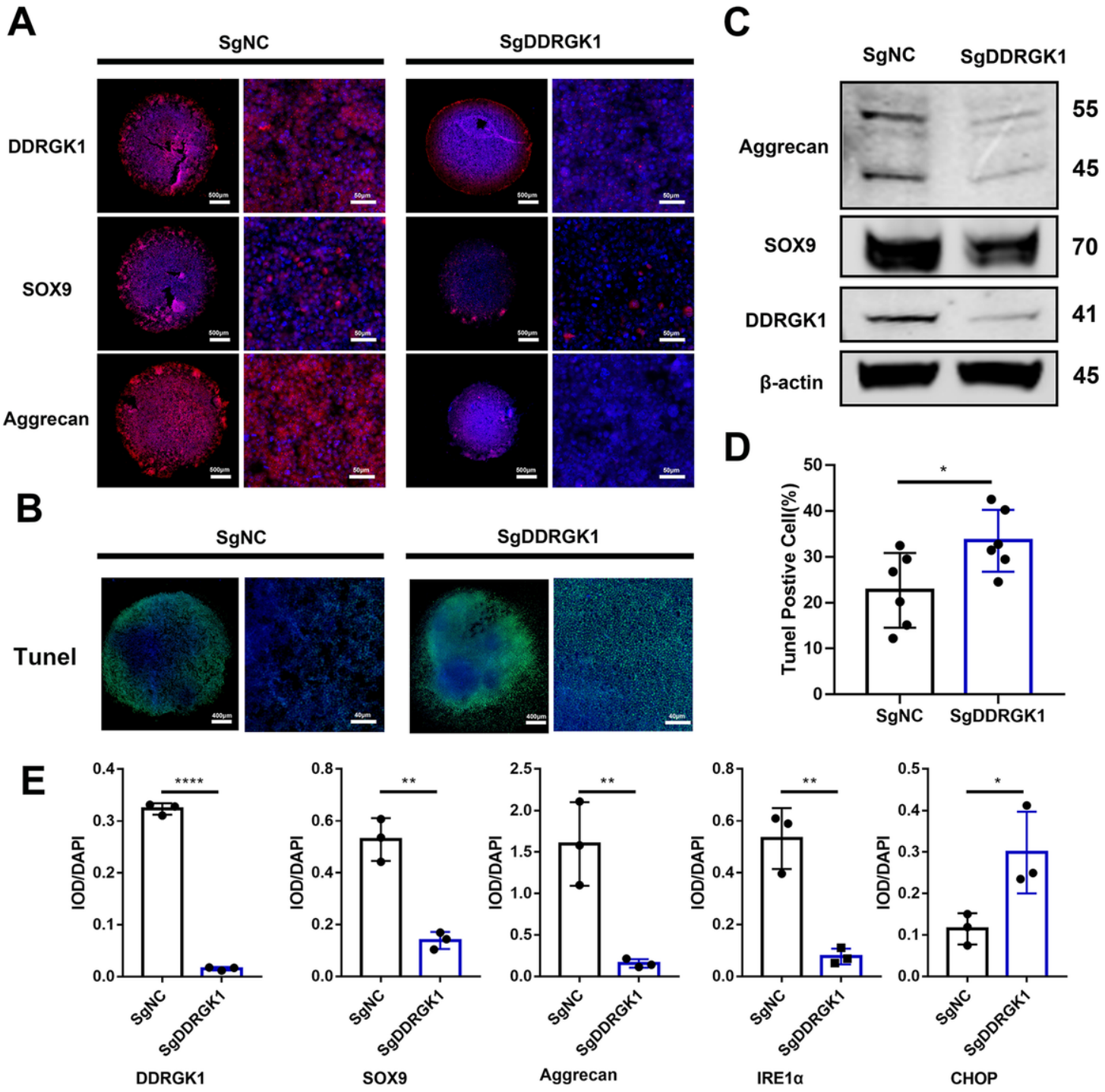

Figure 6

Loss of DDRGK1 impaired chondrogenesis, activated ER stress and induced apoptosis in the ATDC pellet culture. (A) Immunofluorescence analysis of DDRGK1, SOX9 and aggrecan expression in the pellet culture of SgNC and SgDDRGK1 ATDC5 chondrocytes 21 days after culture in chondrogenesis medium. (B)

TUNEL immunofluorescence staining of the pellet culture of SgNC and SgDDRGK1 ATDC5 chondrocytes 21 days after culture in chondrogenesis medium. (C) Western blot analysis of aggrecan, SOX9 and DDRGK1 expression using β-actin as the loading control in SgNC and SgDDRGK1 ATDC5 chondrocytes. (D) Quantification of the percentage of TUNEL-positive cells in the pellets shown in (B). (E) Quantification of the IOD/DAPI levels shown in (A) and Supplementary Figure 5. All data are presented as the mean ± SD. *P < 0.05, **P < 0.01, ***P < 0.001 and ****P < 0.0001.

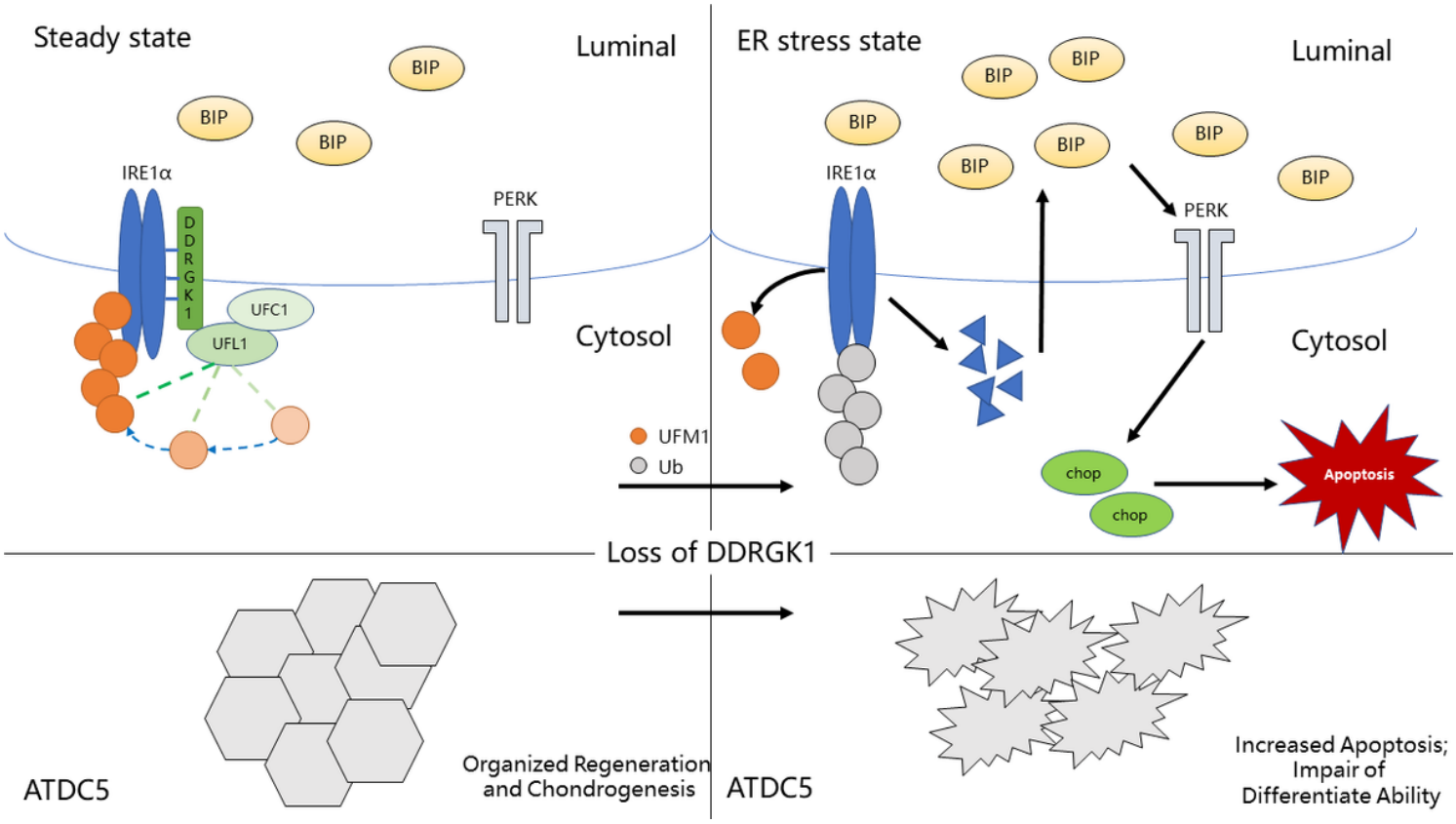

Figure 7

Regulatory function of DDRGK1 in the UFMylation of IRE1α, ER homeostasis, apoptosis and chondrogenesis in ATDC5 chondrocytes. DDRGK1 interacts with IRE1α on multiple sites to facilitate the UFMylation of IRE1α to maintain its stability with the help of UFL1 and UFC1. Loss of DDRGK1 expression impairs the integrity of IRE1α, leading to its ubiquitin-mediated degradation, which activates ER stress, upregulates BiP expression, dimerizes PERK and increases CHOP expression to induce apoptosis in ATDC5 chondrocytes. This in turn reduces their chondrogenic capabilities.

Supplementary Files

This is a list of supplementary files associated with this preprint. Click to download.

- Supplementarymaterial.docx